Anthropocene 34 (2021) 100291

Contents lists available at ScienceDirect

Anthropocene

journal homepage: www.elsevier.com/locate/ancene

Recent global land cover dynamics and implications for soil erosion and carbon losses from deforestation

Xiangping Hu[a,*], Jan Sandstad Næss[a], Cristina Maria Iordan[a], Bo Huang[a], Wenwu Zhao[b], Francesco Cherubini[a]

[a] Industrial Ecology Program, Department of Energy and Process Engineering, Norwegian University of Science and Technology, N-7491, Trondheim, Norway
[b] State Key Laboratory of Earth Surface Processes and Resource Ecology, Faculty of Geographical Science, Beijing Normal University, Beijing, 100875, China

ARTICLE INFO

Article history:
Received 3 November 2020
Received in revised form 12 March 2021
Accepted 24 March 2021
Available online 26 March 2021

Keywords:
Land cover change
Climate change
Deforestation
Land use emissions
Soil erosion

ABSTRACT

Changes in land cover are increasingly affecting land surface properties and provision of ecosystem services. Understanding recent historical land cover changes and their interlinkages with key environmental processes is instrumental to better support strategies for land-use management. The recently released products from the European Space Agency and Copernicus Climate Change Service contain high-resolution (300 m) time series of global land cover maps from 1992 to 2018. This study investigates the land transitions in these products and explores the effects on two key environmental aspects, namely, carbon losses from deforestation and soil erosion rates. We used a powerful server for big data analysis to retain the original spatial resolution of the datasets. We found 722 Mha (5.5 % of the total ice-free land surface) of gross land cover changes, which mainly involved transitions to and from forest/agriculture. Cropland gains are 205 Mha and losses 126 Mha (net expansion of 79 Mha). Deforestation occurring in 242 Mha was mainly caused by agricultural expansion, whereas 196 Mha were afforested. Settlements show the largest relative expansion (44 Mha, +210 %), of which 67 % (29 Mha) occurred at expenses of agricultural land. Deforestation caused 12.3 (7.6/14.2) Gt Carbon losses from below- and aboveground biomass from 2010 to 2018, corresponding to 1.5 (1.0/1.8) Gt Carbon per year. Global agriculture activities have increased total soil erosion of 3.2 Gt and soil erosion rates of 0.22 Mg ha^{-1} yr^{-1} in the period 2001–2012, especially in tropical regions. The identified land transitions and changes in key environmental processes reflect a human-dominated Earth system and the indirect effects of climate change on land cover, especially in boreal ecosystems.

1. Introduction

Land is the basis for human livelihoods and well-being. It is the main supplier of food, freshwater and multiple other ecosystem services, including biodiversity. Human activities are already affecting more than 70 % (likely 69–76 %) of the global, ice-free land surface (IPCC, 2019). Anthropogenic activities have caused extensive land cover changes (Klein Goldewijk et al., 2017), which also affected protected areas within biodiversity hotspots (Bailey et al., 2016; Hu et al., 2020). Changes in land cover are both a driver and a consequence of global environmental change (Foley et al., 2005; Bonan, 2008; Alkama and Cescatti, 2016), and they have great impact on our society and ecosystems at regional and global scales (Verburg et al., 2011; Turner et al., 2007).

Assessing changes in land cover and their environmental effects is an on-going and fast developing research area (Nowosad et al., 2019; Hua et al., 2018; Mousivand and Arsanjani, 2019; Liu et al., 2018b; IPCC, 2019). Major applications aim to understand spatial and temporal patterns of land cover dynamics (IPCC, 2019; Mousivand and Arsanjani, 2019; Liu et al., 2018b), explain the underlying mechanisms causing the changes (Lepers et al., 2005; Ceccherini et al., 2020; Jaimes et al., 2010), construct models for assessing challenges to society and environment (Hurtt et al., 2020; Kuemmerle et al., 2016; Chen et al., 2020), quantify impacts to climate change at a global (Alkama and Cescatti, 2016; Bonan, 2008; Prestele et al., 2017) or regional scale (Huang et al., 2020a; Hu et al., 2019; Lejeune et al., 2018; Cherubini et al., 2018a), assess effects on ecosystem services (Tolessa et al., 2017; Chen et al., 2019; Bayer et al., 2020; Venäläinen et al., 2020), and help stakeholders to design more sustainable land use polices (Ellis and Ramankutty, 2008; Duveiller et al., 2020; Verburg et al., 2011; Seneviratne et al.,

* Corresponding author at: Industrial Ecology Program, Department of Energy and Process Engineering, Norwegian University of Science and Technology, N-7491, Trondheim, Norway.
E-mail address: Xiangping.Hu@ntnu.no (X. Hu).

http://dx.doi.org/10.1016/j.ancene.2021.100291

2018; Englund et al., 2020). Different types of land cover or land use changes have been studied in the literature, such as agriculture expansion and contraction (Grau et al., 2005; Spawn et al., 2019; Krause et al., 2009; Næss et al., 2021; Leirpoll et al., 2021), deforestation and afforestation (Seto et al., 2012; Jaimes et al., 2010; Li et al., 2016; Hansen et al., 2013), forest dynamics and management (Ceccherini et al., 2020; Pan et al., 2011; Hansen et al., 2013; Cherubini et al., 2018b), urbanization (Arsanjani et al., 2013; Cakir et al., 2008; Arsanjani et al., 2018), wetland shrinkage (Song et al., 2012; Ghosh et al., 2018; Debanshi and Pal, 2020; Xu et al., 2019), and desertification (Veron et al., 2006; Bestelmeyer et al., 2015; Lamchin et al., 2016). A common approach used is the temporal analysis of variability per pixel to detect land cover transitions. Results are frequently shown as aggregated averages at relatively low resolution or focus on specific regions and spatial scales. This is due to two main issues that analysts face when assessing changes in land cover at high spatial resolution and global scale. The first is related to the challenges in processing big datasets, because timeseries of high-resolution global datasets with detailed land cover classification are usually highly computationally demanding and time consuming. The second is due to the lack of both spatially and temporarily consistent land cover datasets that cover the globe for a long time period of observations (Nowosad et al., 2019). Recently, the European Space Agency's Climate Change Initiative (ESA–CCI) provided annual global land cover maps from 1992 to 2015, and the Copernicus Climate Change Service climate data store (C3S-CDS) released the global land cover annual maps from 2016 to 2018 (C3S, 2019). These two datasets are highly consistent and have high spatial resolution (300 m at the equator), and they offer the possibility to analyze global land cover transitions in detail.

Some studies have investigated the ESA–CCI land cover product from different perspectives. Li et al. (2016) used an early version of the ESA–CCI land cover product to analyze land transitions at three specific points in time, 2000, 2005 and 2010. However, due to computational challenges, they disregarded some transitions to save resources and time. Liu et al. (2018b) identified land transitions and hotspots of land use changes using the trajectory analysis method. However, again due to limited computation capacity, they had to aggregate the datasets into $0.5^\circ \times 0.5^\circ$ resolution and then compute the area proportions in the aggregated datasets. Li et al. (2018) analyzed the gross and net changes in land covers for some plant functional types commonly used in land surface models. They investigated the spatial distribution of changes in land cover for cropland, grassland and forests between 1992 and 2015. They also compared the ESA–CCI land cover product to the LUH dataset (Hurtt et al., 2011), concluding that the ESA–CCI data can improve the representation of land cover dynamics in land surface models and the characterization of local or global carbon cycle dynamics. Nowosad et al. (2019) assessed and visualized main land cover gains and losses between 1992 and 2015 after pre-processing the land cover data to resize them at a landscape level. The ESA–CCI land cover product was also used by Mousivand and Arsanjani (2019) to quantify historical changes in land covers and then predict future land transitions using Markov chain. Some of these studies apparently did not consider the curvature of the Earth while translating the gridded land cover datasets into areal extensions, and thereby introduced a bias (overestimation) of the areas for the grid cells at high latitudes (Liu et al., 2018a; Mousivand and Arsanjani, 2019; Liu et al., 2018b). Overall, these studies did not include the recent C3S-CDS product (which also includes annual land cover maps from 2016 to 2018), since it was not available at that time, and they did not quantify the specific land cover transitions or their spatial distributions. Preliminary studies are also integrating the ESA–CCI land cover products with adjacent fields, such as remotely sensed data or other ground-level observations to study the effects of changes in land covers on regional climate (Huang et al., 2020a; Duveiller et al., 2018), and, although relatively little explored so far, they offer possibilities for integrations with multiple datasets to discern the effects of changes in land covers on environmental areas of concerns, like for example soil erosion, vegetation carbon storage, and ecosystem services.

In this study, we quantitatively analyze and visualize recent historical land cover dynamics at a global level from 1992 to 2018 as represented by the integration of the ESA–CCI and C3S-CDS land cover products. The analysis retains the original spatial resolution (300 m) of the maps thanks to the use of a powerful server for big data analysis, and it shows gains and losses in land cover, as well as trends and spatial patterns of land cover transitions (i.e., from one land cover class to another). The 37 original land cover classes of the datasets are translated into the land cover classes specified by the Intergovernmental Panel on Climate Change (IPCC), which are

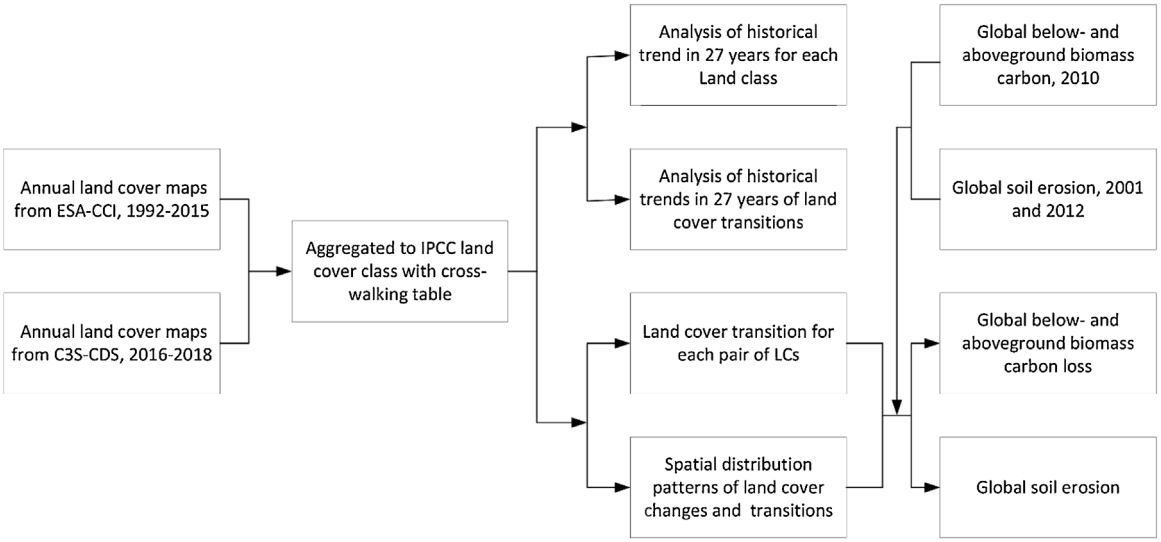

Fig. 1. A simplified flowchart of the approach and main methodological steps considered in this study, from the original datasets to the estimates of carbon emissions from vegetation losses and soil erosion.

more reliable for the identification of land cover transitions than the original classes.

To the best of our knowledge, this is the first attempt to merge and analyze the two land cover products, to show global maps and timeseries of both changes in land covers (losses and gains) and land transitions between each pair of land cover classes, and to identify areas of potential hotspots of changes in land covers at a global level. In addition, we apply this integrated dataset to assess the effects of historical recent changes in land covers on two major global environmental issues: total carbon emissions and their spatial patterns from losses in aboveground and belowground biomass carbon due to deforestation to agriculture and settlement; contribution to global soil erosion from land use (i.e., agriculture) and changes in land covers (e.g., from forest to agriculture and vice versa). Fig. 1 shows a simplified flowchart of the approach and main methodological steps considered in the study.

In summary, the aim of our work is to address the following research questions:

- What are the main global land transitions from 1992 to 2018 according to the ESA–CCI and C3SCDS products?
- What are the spatial distributions of the main land cover transitions?
- How does global land cover and land use changes influence key environmental aspects, such as carbon losses from deforestation and soil erosion rates?

2. Methodology

2.1. Land cover datasets

The land cover products from ESA–CCI and C3S-CDS provide global annual maps from 1992 to 2015 and from 2016 to 2018, respectively (ESA, 2017; C3S, 2019), that are highly consistent over time and space. They were specifically developed to provide a consistent evaluation of the historical temporal evolution of changes in land covers at a global level. To ensure the continuity, these two datasets have the same spatial resolution (300 m at the equator, or 10 arc-sec), and each map is in the form of 129600 × 64800 grids Lon/Lat raster. Both products use the World Geodetic System 84 (WGS84) reference ellipsoid as the coordinate reference system, and they provide global maps describing the land surface using the same categories and coding scheme. These datasets have been developed to increase the robustness of land cover datasets for carbon and climate change models, land surface studies, and landscape dynamic assessment (ESA, 2017; C3S, 2019; Li et al., 2018, 2016).

The datasets are based on 37 land cover classes according to the United Nations Land Cover Classification System to describe the Earth's terrestrial surface (Di Gregorio, 2016). These maps are obtained by combining several earth observation products and by using the GlobCover unsupervised classification chain (ESA, 2017; Defourny et al., 2009; Poulter et al., 2015). Unlike the other single-year products, the land cover products from ESA–CCI and C3S-CDS maintain good time consistency, and their overall global accuracy is about 71 % (ESA, 2017; C3S, 2019). Some classes, such as cropland, forests, urban and bare areas have higher accuracy, and others, such as mosaic classes, have lower accuracy. The high certainty of cropland classes makes the land cover products especially useful for cropland monitoring. Global user and producer accuracies of cropland classes range between 85–94 % and 76–92 % across both datasets, with medians of 89 % and 82 % (ESA, 2017; C3S, 2019). These high user and producer accuracies indicate a high spatial cropland match and high precision in total cropland area extent. Additionally, broadleaved evergreen forests have high user and producer accuracies (86 % and 96 % for ESA–CCI, and 89 % and 86 % for C3SC-CDS, respectively), thereby making the products suitable for monitoring tropical deforestation and afforestation. For example, ESA–CCI has a regional overall accuracy of 85 % when applied as a forest product in the Brazilian Amazon (Qin et al., 2019).

The original 37 land cover classes in these two land cover products have been translated into the generic IPCC land cover classes with a cross-walking table (Supplementary Table S1) to obtain more reliable results of land cover transition dynamics (ESA, 2017). This conversion avoids false change detection between land cover classes which are semantically close in the original 37 land cover classes (ESA, 2017; Liu et al., 2018b). The ESA–CCI land cover product has already been used to investigate the pattern of changes in land covers (Nowosad et al., 2019; Tschora and Cherubini, 2020; Liu et al., 2018b), to assess consistency with other products (Hua et al., 2018; Liu et al., 2018a) and to investigate climate-land interactions (Duveiller et al., 2018; Huang et al., 2020a; Li et al., 2018). However, to the best of our knowledge, these two land cover products have not been integrated into a single dataset and the spatial patterns at a global level have not been depicted.

2.2. Datasets of global biomass carbon and soil erosion

A harmonized global dataset of biomass carbon density, aboveground (ABC) and belowground (BBC), for 2010 at 300 m resolution has been recently made available (Spawn and Gibbs, 2020; Spawn et al., 2020), and it is here used to quantify gross vegetation carbon losses due to the major land use transitions that happened between 2010 and 2018. This carbon density map was created with a novel method that integrates remotely sensed maps of specific vegetation characteristics with ancillary maps of tree cover, land covers and rule-based decision tree (Spawn et al., 2020). The dataset combines published estimates for vegetation specific densities and their results have been rigorously validated. The dataset was recently built from the ESA–CCI product, and it has the same resolution of the two land cover datasets used in our study.

Land cover transitions and anthropogenic activities are among the main causes of soil erosion (SE), which lead to serious consequences to human society, such as risks to food security and depletion of ecosystem services (Borrelli et al., 2017; Tarolli and Straffelini, 2020; Huang et al., 2020b). SE is usually defined as the mass of net soil loss per unit area and time (Nearing et al., 2017b). Borrelli et al. (2017) provided a resampled global dataset of SE rates in 2001 and 2012, with a spatial resolution of 25 km, to study temporal changes in soil erosion rates over time. Their estimates of SE rates are based on the revised universal soil loss equation (RUSLE) modelling approach, a well-known empirical method for predicting SE (Risse et al., 1993; Stolpe, 2005; Bagarello et al., 2017). In the RUSLE approach, SE is expressed as the mass of soil loss per unit area and time and computed by combining the contribution factors, such as land cover and management, rainfall runoff erosivity, soil erodibility, slope steepness and length, and soil conservation practice. This dataset was produced to investigate the nexus between land cover transitions and SE, especially to monitor the risks of increasing SE rates due to cropland expansion. For example, Borrelli et al. (2017) showed a global increase in soil erosion driven by land use change of 2.5 % between 2001 and 2012.

All these datasets are converted to the same spatial resolution of the land cover data, i.e., 300 m. If the original maps do not cover the whole globe, they are extended to cover -90 °N -90 °N and -180 °E -180 °E, and values of pixels in the extended parts are marked as missing values.

2.3. Analysis of land cover dynamics

To answer the first and second research questions of this study, we combined the ESA–CCI and the C3S-CDS land cover products to investigate the historical land cover dynamics from 1992 to 2018. Our main focus is on total change and trend of each land cover class, land transitions between different land covers, and spatial distributions of the observed land dynamics. We firstly computed the total area of each grid for each specific IPCC land cover class, considering the curvature of the earth. The total area for each land cover class m (denoted as $Area_m$) is computed as follows,

$$Area_m = \sum_{j=1}^{N} (LC_j = m) \times A_j \tag{1}$$

for every year from 1992 to 2018. j is the index of the grid with a spatial resolution of 300 m at the equator, and LC_j is the land cover class in grid j. N denotes the total number of grids on the whole Earth. A_j is the area of grid j, which varies by latitude: 0.09 km^2 at the equator and gradually smaller while progressing towards the pole because of the curvature of the Earth. The latter is taken into account as follows,

$$A_j = \frac{\pi}{180} \times R^2 \times |\sin(lat_2) - \sin(lat_1)| \times |lon_2 - lon_1| \tag{2}$$

where, R is the Earth radius, lat_1, lat_2, lon_1 and lon_2, are the values of latitude and longitude of grid A_j, and $|\bullet|$ stands for the absolute value. To better illustrate the global trends of changes in each land cover class, results from Eq. (1) are normalized to the total area in 1992 of each land cover type.

We then investigate the pairwise land cover transitions (denoted as $LC_{m,Yearp\rightarrow n,Yearq}$) between two years to see if a grid changed the land cover class (e.g., from m to n),

$$LC_{m,Yearp\rightarrow n,Yearq} = (LC_j = m)_{Yearp} \times (LC_j = n)_{Yearq} \tag{3}$$

where, $LC_{m,Yearp\rightarrow n,Yearq}$ is a matrix with 0 and 1 to indicate the transition of land cover class m in year p (denoted as $Yearp$) to land cover class n in year q (denoted as $Yearq$) for all pairs of m and n, $m \neq n$. The total area of the transition between the two years (denoted as $Area_{m,Yearp\rightarrow n,Yearq}$) is computed by combining Eqs. (2) and (3) as follows

$$Area_{m,Yearp\rightarrow n,Yearq} = \sum_{j=1}^{N} LC_{m,Yearp\rightarrow n,Yearq} \times A_j \tag{4}$$

Eq. (4) can be used to compute the total area of pairwise land cover transitions for any given two years between 1992 and 2018. The global land cover transitions are identified and then aggregated to 9 km spatial resolution at the equator by a local window of 30-by-30 grids for map visualization purposes. The area proportion (from 0 to 1) of each land cover transition (denoted as $AreaP_{m,Yearp\rightarrow n,Year}$) between any chosen two years in each local window is computed as

$$AreaP_{m,Yearp\rightarrow n,Yearq} = \frac{\left(\sum_{j=1}^{P} (LC_j = m)_{Yearp} \times (LC_j = n)_{Yearq} \times A_j\right)}{\sum_{j=1}^{P} A_j} \tag{5}$$

Both sums in numerator and denominator in Eq. (5) are within the local window, which contains 900 grids, i.e., P = 900. Different low spatial resolutions can be obtained through Eq. (5) if necessary.

The changes in land covers can be obtained similarly. First, we identified the land cover increase or decrease (denoted as $LC_{j,m\uparrow,Yearp}$ and $LC_{j,m\downarrow,Yearq}$, respectively) for grid j and each land cover class m between any given two years between 1992 and 2018,

$$\begin{aligned} LC_{j,m\uparrow,Yearp\rightarrow Yearq} &= (LC_j \neq m)_{Yearp} \times (LC_j = m)_{Yearq} \\ LC_{j,m\downarrow,Yearp\rightarrow Yearq} &= -(LC_j = m)_{Yearp} \times (LC_j \neq m)_{Yearq} \end{aligned} \tag{6}$$

Using Eq. (6), the increase and decrease of each land cover are coded as 1 and -1. If there is no change between the two years, we set the value of the grid to 0. Using this approach, the spatial distribution patterns of the changes in land covers can be obtained. We then aggregated the result to 9 km spatial resolution using a local window of 30-by-30 grids for visualization purposes,

$$AreaP_m = \frac{\left(\sum_{j=1}^{P} (LC_{j,m\uparrow,Yearp\rightarrow Yearq} + LC_{j,m\downarrow,Yearp\rightarrow Yearq}) \times A_j\right)}{\sum_{j=1}^{P} A_j} \tag{7}$$

Similar to Eq. (5), both sums in numerator and denominator in Eq. (7) are within the local window.

2.4. Estimates of carbon losses and soil erosion

To answer the third research question of this study, we estimated the biomass carbon losses and SE due to land cover transitions. The loss of biomass carbon due to loss in forest cover for the transition from forest to agriculture or settlement is estimated from the global ABC and BBC density datasets recently made available (data are representative of 2010 only) (Spawn et al., 2020). The ABC loss due to deforestation (forest to agriculture, denoted as $\Delta\, ABC_{FOR\rightarrow AGR}$) is computed by identifying the grids of forest areas in 2010 that have been converted to agriculture in 2018, assuming the difference in aboveground biomass between the two land covers as an instantaneous emission to the atmosphere. For these grids, carbon emissions are estimated by the difference between the associated ABC content of forests in each grid transitioned to agriculture and the global average carbon content of agricultural land, as follows

$$\Delta ABC_{FOR\rightarrow AGR} = \sum_{g} \left(ABC_{g,FOR,2010} - ABC_{AGR}\right) \times A_g \tag{8}$$

where, ABC_{AGR} is the estimated average ABC density per grid cell g of all agricultural grids. This is done to consider average carbon density for agricultural land, because the ABC density for 2010 is not available (as the grid was classified as forest). ABC_{AGR} is assumed to be equal to the global mean, the 10th percentile or the 90th percentile of all ABC of agricultural grids in 2010. The sum in Eq. (8) computes the total carbon emissions from all the grids that were classified as forest in 2010 and agriculture in 2018. Similarly, the estimated ABC loss for forest to settlement ($\Delta\, ABC_{FOR\rightarrow SET}$) is computed as

$$\Delta ABC_{FOR\rightarrow SET} = \sum_{h} ABC_{h,FOR,2010} \times A_h \tag{9}$$

under the assumption that deforestation to settlement leads to a total loss of ABC. The sum in Eq. (9) estimates total carbon emissions from all the grids h that were classified as forest in 2010 but settlement in 2018. Eq. (3) can be used to identify the transitions in Eqs. (8) and (9). It was then possible to produce maps of the loss of ABC and show the main emission regions, after aggregation to local windows of 30-by-30 grids that include the sum of the therein loss of ABC to improve visualization. The same procedure is used to estimate carbon losses from belowground biomass carbon, but in this case the BBC density maps are used.

Similarly, we study SE associated with the main land cover transitions by integrating the SE dataset and the land cover

products. The SE dataset provided by Borrelli et al. (2017) contains the SE rates in two years, 2001 and 2012 (denoted as SER_{2001} and SER_{2012}). Under the assumption that the SE rate changes linearly during these two years, the rate of change of the SE rates in each grid k can be computed as

$$b_{k,m\to n} = \frac{SER_{k,m,2012} - SER_{k,n,2001}}{\Delta t} \quad (10)$$

with $\Delta t = 11$. With 2001 as the reference year ($t = 0$), the total increased SE from 2001 to 2012 (denoted as $\Delta SE_{m,2001\to n,2012}$) can be computed as

$$\begin{aligned} \Delta SE_{m,2001\to n,2012} &= \sum_k \int_{t=0}^{t=11} b_{k,m\to n} t dt \times A_k \\ &= \frac{11}{2} \sum_k A_k \times \left(SER_{k,m,2012} - SER_{k,n,2001}\right) \end{aligned} \quad (11)$$

The sum in Eq. (11) is over each grid k which is classified as land cover class m in 2001 and class n in 2012, and $m = n$ is allowed. Such a setting enables us to compute the SE not only due to land cover or land use change, but also for the same land cover over time. In this study we focus on SE due to land cover transitions between agriculture and forest, agriculture remaining agriculture, and forest remaining forest.

3. Results

3.1. Global trends of land cover changes

The trends in recent historical changes for each type of land cover class are shown in Fig. 2, the underlying losses, and gains in Supplementary Figure S1, and the main transitions between pairs of land cover classes in Fig. 3. Results are normalized to the relative area of each land cover class in 1992.

In relative terms, settlement is by far the land cover class that increased the most during the study period, as it has expanded by more than 200 % (Fig. 2b). The second largest increase (3%) is for agriculture, whose net area gains peaked around 2006 and then remained relatively constant (Fig. 2a). However, this stable trend does not imply that there were no transitions to and from agriculture and other land cover classes (mainly forest) after 2006, because it is the result of a balance between agriculture gains and losses (Fig. S1). Until 2006, conversion of forests to agriculture was larger than the opposite transition (from agriculture to forests), resulting in net area gains for agriculture, but after 2006 the two transitions are approximately of the same magnitude (Fig. 3a). Grassland areas expand of about 1% (Fig. 2a), and this is largely at expenses of forest areas (Fig. 3b). All other land covers have decreased with varying trends. Wetland had the most significant decreasing trend (-6%), mainly as a result of drying due to climate change, unsustainable water withdrawals, and excessive nutrient loads that favor plant growth (Werner et al., 2013; Green et al., 2017), which make vegetation to gradually take over wetland areas (Fig. 3c). Shrubland and sparse vegetation decreased steadily from 1992 to 2008 (-2%), and thereafter the net trends remained relatively constant. Changes in area extensions of shrubland and sparse vegetation are difficult to interpret. Shrubland in tropical areas can be typically associated with savannah or Cerrado, and the shrubland-to-forest transition can indicate a development of early-stage trees in 1992 that are progressively becoming larger and with closer canopy. The opposite transition (forest-to-shrubland) can be indicative of forest degradation (Fig. 3d). Net changes of forest areas show a decline of 1%, which mainly occurred before 1999, but declines in forest areas are still on-going (although compensated by forest expansion). Bare areas are also declining in favor of grassland, a transition that can be explained by the progressive observed greening of the Earth as a feedback to rising atmospheric carbon concentrations and temperatures (Zhu et al., 2016).

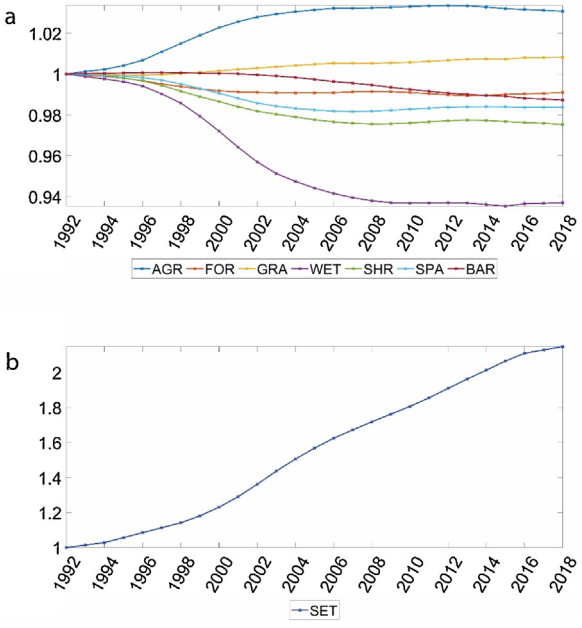

Fig. 2. Normalized trends for each land cover from 1992 to 2018. Different colors indicate different classes. Trends are smoothed using a five-year moving average. (a) Normalized trends for agriculture, forest, grassland, wetland, shrubland, sparse vegetation, and bare areas. (b) Normalized trends for settlement. AGR: Agriculture, FOR: Forest, GRA: Grassland, WET: Wetland, SET: Settlement, SHR: Shrubland, SPA: Sparse vegetation, BAR: Bare area.

3.2. Total land cover changes and spatial distributions

The total changes in land covers from the beginning (1992) to the end (2018) of our study period are quantified in terms of million hectares (Mha) and shown in Table 1 (numbers in the table refer to the transitions from row to column). There are transitions among all land classes, except from settlement to other classes. The global spatial distribution of the patterns of relative gains and losses for each land cover and the main land cover transitions are shown in Figs. 4 and 5, respectively.

A total of 722 Mha of gross changes in land covers occurred in our planet between 1992 and 2018 according to the ESA–CCI and C3S-CDS datasets. Agriculture is the land cover class with the largest area gains (205 Mha) and forest the one with the largest decrease (241 Mha). At the same time, agricultural has lost 126 Mha and forest has gained 196 Mha, resulting in net area changes of +79 Mha and −45 Mha, respectively. Agriculture mainly translated to forests (79 Mha), a transition that is typically associated with either cropland abandonment due to socio-economic reasons, such as in Eastern Europe after the fall of the Soviet Union (Lesiv et al., 2018), or afforestation for ecological restoration, such as in coastal Brazil (Rezende et al., 2018), or measure to contrast land degradation, such as in China (Peng et al., 2014). These regions of the world are among those that show the main trends in agricultural declines and increases in forest areas (Fig. 4a, b and Fig. 5a). Settlement is the second main driver of agriculture area loss (29 Mha, about 23 % of the total agriculture loss), and mostly occurred in Eastern China, India, US, and Western Europe (Fig. 5b). Agriculture expansion mainly happened at expenses of forest (123 Mha), shrubland (30 Mha) and grassland (25.7 Mha), and essentially took place in many world regions, such as Central and Eastern Asia, US, South America, and Central Africa (Fig. 4a). The largest presence of forest-to-agriculture transitions occurred at the borders of the Amazon basin and in Southeast Asia

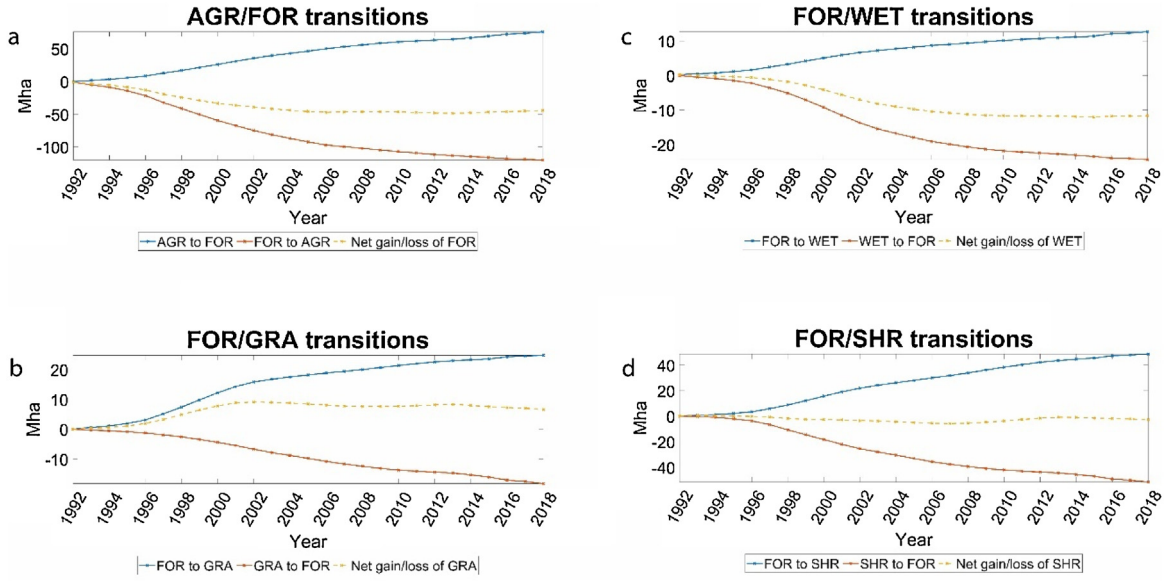

Fig. 3. Land cover transitions, in million hectares (Mha). Trends are smoothed using a five-year moving average. (a) Agriculture/Forest transitions. The blue line shows the transition from agriculture to forest, and the red line shows the transition from forest to agriculture. The yellow line is the net gain or loss of forest in forest/agriculture transitions. (b) Forest/Grassland transitions. The blue line shows the transition from forest to grassland, and the red line shows the transition from grassland to forest. The yellow line is the net gain or loss of grassland in forest/grassland transitions. (c) Forest/Wetland transitions. The blue line shows the transition from forest to wetland, and the red line shows the transition from wetland to forest. The yellow line is the net gain or loss of wetland in forest/wetland transitions. (d) Forest/Shrubland transitions. The blue line shows the transition from forest to shrubland, and the red line shows the transition from shrubland to forest. The yellow line is the net gain or loss of forest in forest/shrubland transitions. AGR: Agriculture, FOR: Forest, GRA: Grassland, WET: Wetland, SET: Settlement, SHR: Shrubland, SPA: Sparse vegetation, BAR: Bare area.

Table 1
Global land cover changes during the period 1992-2018. The numbers in the table refer to the transitions from row to column. AGR: Agriculture, FOR: Forest, GRA: Grassland, WET: Wetland, SET: Settlement, SHR: Shrubland, SPA: Sparse vegetation, BAR: Bare area, WAT: water (Unit: Mha).

	AGR	FOR	GRA	WET	SET	SHR	SPA	BAR	WAT	Sum (loss)
AGR	0	79.0	9.2	0.2	29.1	4.0	1.7	1.2	1.8	126.2
FOR	123.7	0	26.6	14.4	4.3	52.1	9.0	2.6	8.9	241.5
GRA	25.7	19.4	0	0.3	4.7	1.5	20.1	6.9	1.0	79.5
WET	1.1	24.7	0.6	0	0.3	0.4	0.3	0.0	1.4	29.0
SET	0	0	0	0	0	0	0	0	0	0
SHR	30.1	54.4	3.8	0.2	2.2	0	1.2	0.5	0.5	93.0
SPA	18.7	13.6	33.6	0.3	0.7	0.7	0	12.4	0.6	80.7
BAR	4.7	0.4	19.6	0.0	2.0	0.1	29.7	0	0.9	57.4
WAT	1.4	4.4	0.8	2.3	0.4	0.5	0.7	4.6	0	15.0
Sum (gain)	205.2	196.0	94.3	17.7	43.7	59.3	62.7	28.2	15.1	722.2
Net (gain-loss)	79.1	−45.5	14.8	−11.3	43.7	−33.7	−18.0	−29.2	0.2	

(Fig. 5c). Global deforestation resulted in a loss of forest area equal to 241 Mha. After agriculture, the main forest losses are caused by shrubland (52 Mha) and grassland (27 Mha), detected in South America and the boreal climate (Fig. 5d). Agriculture, shrubland, and grassland together are responsible for 84 % of forest loss. Expansion of forest areas mainly come from agriculture (79 Mha), shrubland (54 Mha) and wetland (25 Mha). These transitions are mostly due to the effects discussed above, such as cropland abandonment and afforestation programs in the case of agriculture-to-forest (Fig. 5a), forest degradation or potential inconsistencies in the classification system for the shrubland-to-forest, and global warming and/or anthropogenic activities for wetland-to-forest (Fig. 5e). There are multiple other possible considerations for the changes in land covers and transitions among the different classes. Grassland major gains are from sparse vegetation (34 Mha), forest (27 Mha) and bare areas (20 Mha). The latter mostly occurred in arid and semi-arid areas (Fig. 5g). Shrubland largely increased at expenses of forests (52 Mha), and settlement mostly took over agricultural land (29 Mha, 67 % of the total expansion) (Fig. 5b). Further, settlement appears to be a non-reversible land cover class in the datasets considered in our analysis, because no conversion of settlement to other land cover classes is registered throughout the whole study period. Sparse vegetation mainly originated from bare areas (30 Mha) and grassland (20 Mha), which can be correlated to a feedback of warmer conditions and higher CO_2 atmospheric concentrations that extend the growing season and stimulate vegetation activities and tree growth, especially at higher latitudes (Fig. 5h). Similarly, sparse vegetation in boreal climates are also transitioning to forests, as a result of generally improved conditions for tree growth and woody encroachment at forest-tundra ecotones (Fig. 5f). As expected, wetland losses (29 Mha) mainly occurred at high latitudes, especially in the Nordic region and Russia (Fig. 5d), and mainly resulted in expansion of forests. Overall, bare area decreases of 57 Mha, with a net loss of 29 Mha. Bare area loses 30 Mha and 20 Mha to sparse vegetation and grassland, respectively (Figs. 5g and h).

3.3. Global vegetation carbon losses and soil erosion

The global biomass density maps from Spawn et al. (2020) and Spawn and Gibbs (2020) have the same spatial resolution of the land cover products from ESA–CCI and C3S-CDS, and they can be

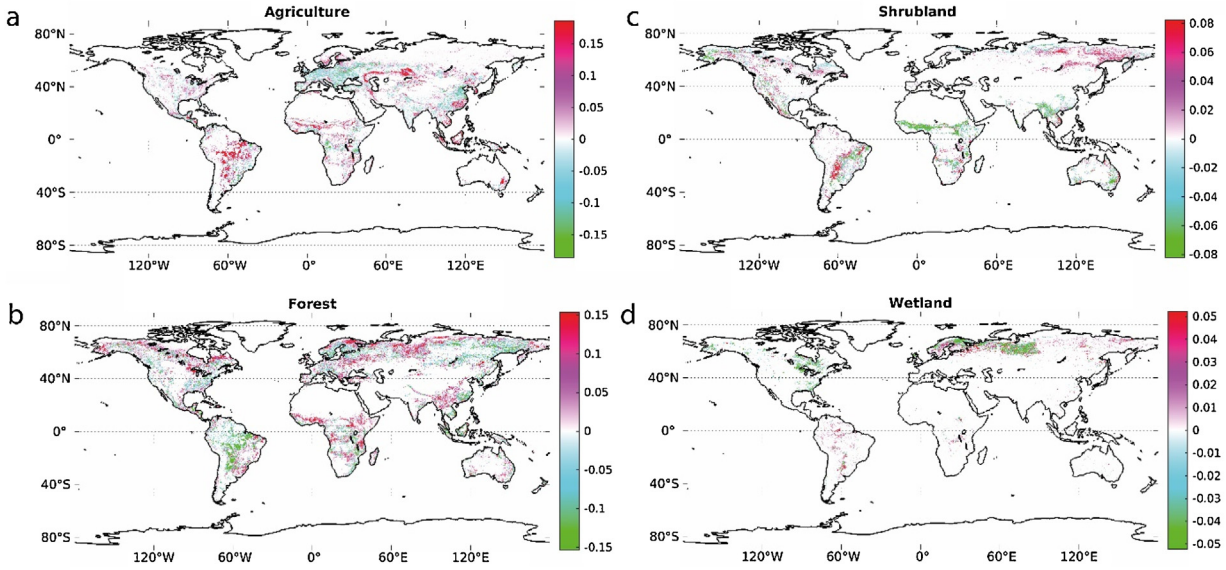

Fig. 4. Global land cover changes (increase or decrease) for selected land cover classes as a fraction of a grid cell. All the subfigures are aggregated to 9 km spatial resolution for visualization purposes only and the numbers in the color bars indicate the fraction of the grid cell affected by the change (positive values indicate expansion, negative values contraction). Land cover change of (a) agriculture, (b) forest, (c) shrubland, (d) wetland. Note different scales on color bars.

integrated to investigate the biomass carbon losses aboveground (ABC) and belowground (BBC) due to the recent historical land cover transitions. In this paper, we focused on the gross global losses due to the transitions from forest to agriculture and settlement. Between 2010 and 2018, we estimated that 9 GtC (5.7/10.7 GtC, when the 90th/10th percentile is used in Eq. (8)) are lost from aboveground vegetation clearance driven by agriculture expansion, and 0.23 GtC are lost from conversion of forest to settlements. The spatial distribution of the ABC loss due to agriculture expansion in forest areas is shown in Fig. 6. The major losses are in the tropical band, mainly South America, Africa, and Indonesia, and are estimated at 6.5 (4.0/8.1) GtC. In the tropics, deforestation rates are high and trees typically store a larger amount of carbon than in other biomes. In terms of BBC, losses follow the same spatial pattern of ABC (see Supplementary Fig. S2), although quantities are smaller. A total of 2.7 (1.8/3.3) GtC is estimated at a global level, and 1.7 (1.1/2.1) GtC in the tropics. Supplementary Table S2 shows specific values.

Average SE rates increased from 5.0 Mg ha^{-1} yr^{-1} in 2001 to 5.2 Mg ha^{-1} yr^{-1} in 2012 in the grid cells that were classified as agriculture in both years (AGR-AGR). The SE rate thus increased 0.23 Mg ha^{-1} yr^{-1} (Table 2), a value that is more than 5 times higher the rate of the forest areas that remained forested (0.041 Mg ha^{-1} yr^{-1}), i.e., grid cells that were classified as forest both in 2001 and 2012 (FOR-FOR). The transition from forest to agriculture (FOR-AGR, grid cells that were classified as forest in 2001 but agriculture in 2012) accelerated SE with an average increase of 0.71 Mg ha^{-1} yr^{-1}, which was 17 times higher than the rate of grid cells where forests remained forests. These changes in rates of soil erosion resulted in a total increase of SE of 3.2 Gt and 1.1 Gt in the AGR-AGR and FOR-FOR case, respectively. Transition from forest to agriculture has caused a total soil erosion loss of 0.14 Gt. Despite the smaller rates, the total SE is larger in FOR-FOR than in FOR-AGR because the former occurs over a much larger area of the globe than the latter. The average SE rate after afforestation of agriculture land (AGR-FOR, i.e., grid cells that were classified as agriculture in 2001 but forest in 2012) is 0.095 Mg ha^{-1} yr^{-1}, which is much lower than the case where agriculture remained agriculture (AGR-AGR). These results confirm the effectiveness of forest establishment as a measure to contrast soil erosion. Large-scale afforestation programs have been implemented in the last 20 years to prevent (or even reverse) land degradation, such as those in the Loess Plateau in China (Feng et al., 2020, 2016).

Global SE caused by agricultural activities (AGR-AGR) mainly occurred in the tropical band, such as Brazil, Sub-Saharan Africa and Southeast Asia (Fig. 7). Decreased rates in SE were found in areas corresponding to countries with transitioning or advanced economies, such as North America, Europe and East China (Fig. 7), where agriculture conservation practices are more common (Borrelli et al., 2017). While declines of SEs in forests can be attributed to climatic variables (and to some extent to forest management), agricultural land areas are more exposed to soil erosion from anthropogenic factors (e.g., tillage). An expansion of practices of conservation agriculture in developing countries is seen as an option to mitigate most of the major negative trends of SE, and ultimately prevent further deforestation from expansion of agricultural areas (Borrelli et al., 2020; IPCC, 2019; Smith et al., 2020).

4. Discussion

This paper performed an extensive quantitative analysis of global land cover dynamics using the 27 years' time series high resolution maps from the ESA–CCI and C3S-CDS products. This overview depicts the major trends in changes in land covers in our planet. The spatial distribution patterns of land cover dynamics shown in this study are broadly in line with those previously reported. For example, Li et al. (2018) found net forest losses between 1992 and 2015 of about 60 Mha (45.5 Mha in our study), mainly occurring in South America, Central America and Indonesia. A study that used satellite data to investigate global land transitions between 1982–2016 for highly aggregated land cover classes, such as tall vegetation (i.e., trees ≥5 m in height), short vegetation and bare ground, found declines in bare ground of 116 Mha (57 Mha in our study, but for a shorter time period), increases in tree cover and reductions in short vegetation (estimates not directly comparable with our study due to different land classification systems) (Song et al., 2018). They also found clear regional patterns in land use changes, such as tropical deforestation, agricultural expansion, temperate reforestation or

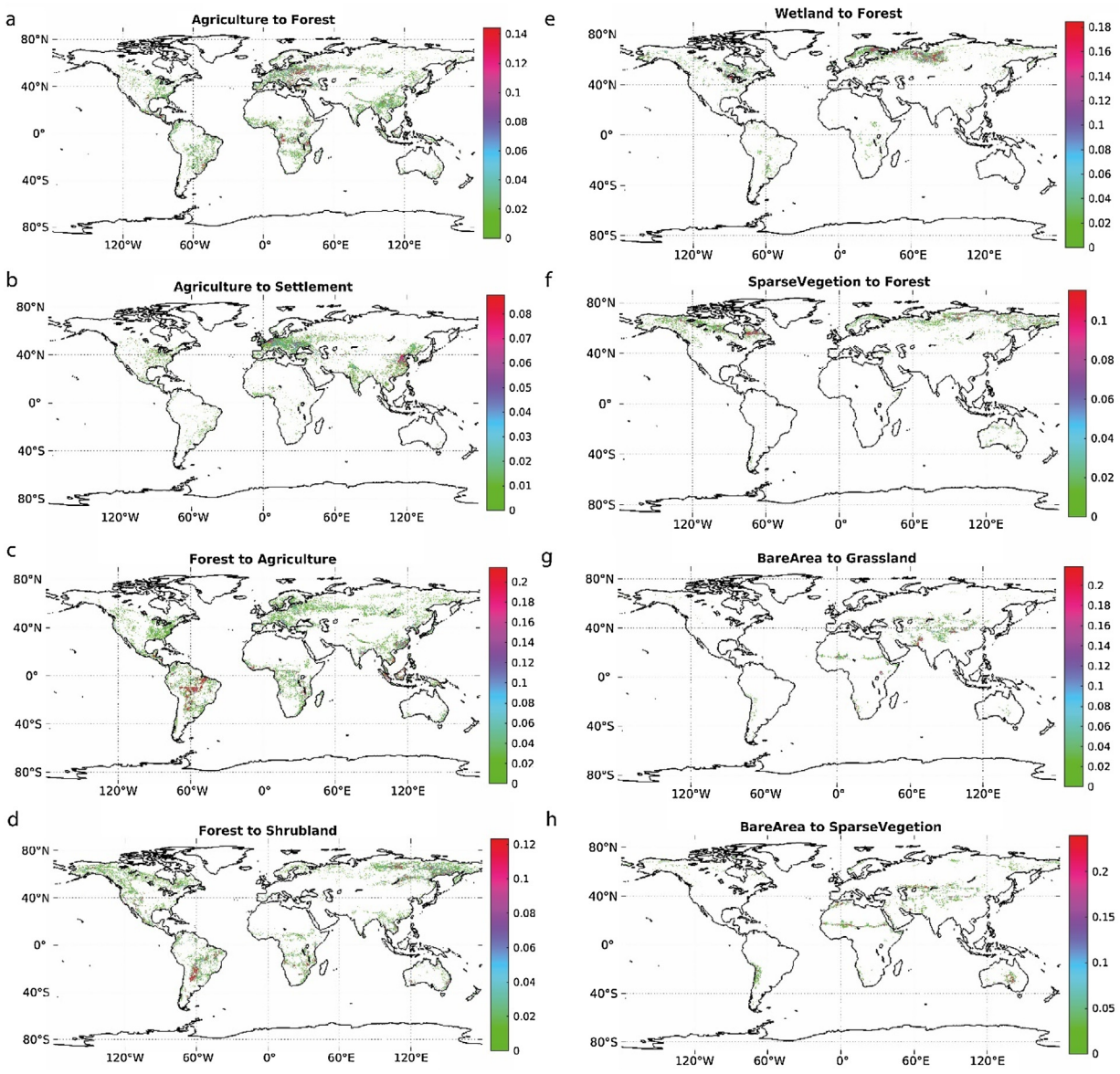

Fig. 5. Global spatial distribution of main land transitions. All the subfigures are aggregated to 9 km spatial resolution for visualization purposes only and the numbers in the color bars indicate the fraction of the grid cell affected by the transition. Transition from agriculture to forest (a), from agriculture to settlement (b), from forest to agriculture (c), from forest to shrubland (d), from wetland to forest (e), from sparse vegetation to forest (f), from bare area to grassland (g), from bare are to sparse vegetation (h). Note different scales on color bars.

afforestation, urbanization, tree cover expansion in northern and montane systems, and vegetation losses in many arid and semi-arid ecosystems.

Previous studies have validated and assessed the accuracy of the land cover data used in our analysis (Li et al., 2018; Hua et al., 2018; Liu et al., 2018a; Defourny et al., 2009). There are limitations in the ESA–CCI and C3S–CCI land cover products, mainly due to potential misclassifications. Global overall accuracies of the two land cover products are 71 % and vary with spatial location and between classes. Regional overall accuracies are found to be 70 % in South America (Pérez-Hoyos et al., 2017), 62 % in Africa (Pérez-Hoyos et al., 2017), 72 % in China (Yang et al., 2017), 84 % in coastal Eurasia (Hou and Hou, 2019), and 64 % in the Arctic (Liang et al., 2019). While the products have relatively high global accuracies for cropland, forests, and urban classes, there are relatively larger uncertainties related to the mapping of mosaic natural vegetation, mosses and lichen classes. This means that our analysis offers more reliable data for the land cover transitions involving forests, agriculture, and settlements, while it has larger uncertainties for the land classes shrubland and sparse vegetation. Additionally, accuracies of individual classes vary slightly across the two land cover products. For example, in the ESA–CCI product, the urban class globally has a higher than average user accuracy (88 %) and a lower than average producer accuracy (51 %), leading to a global underestimation of urban areas. However, this has been improved in C3S-CDS where both urban user and producer accuracies are above average (75 %), providing improved precision in total area extent.

We found that most transitions occurred between forest and agriculture, and agriculture extension was the main driving force of deforestation. Agriculture had the largest net gains during the study period (Table 1), and this is mainly because of the expansion of agriculture activities in Brazil, Africa, Central Asia, Eastern China and Southeast Asia (Fig. 5). This can indicate an increasing demand for food products from developing countries, which is associated with higher risks of conversion to cropland or pasture of forest or shrubland areas. On the contrary, agriculture land is declining in

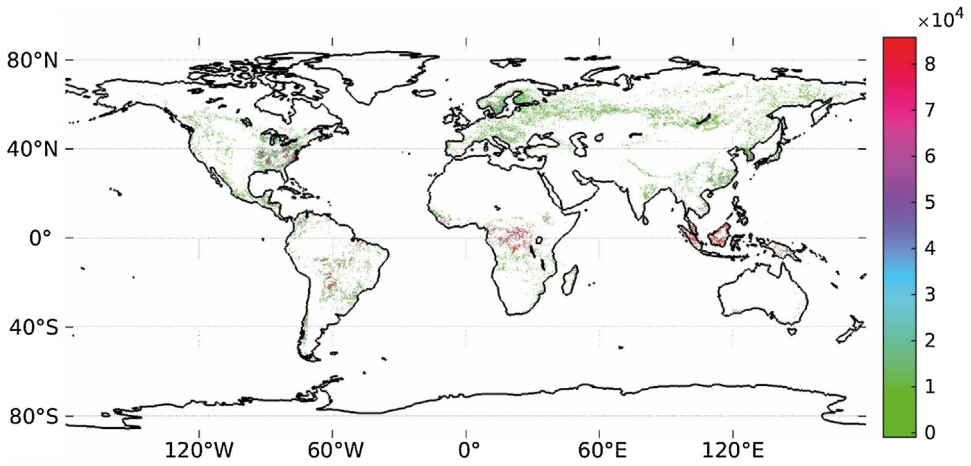

Fig. 6. Spatial distribution of the ABC loss (unit: tC) from 2010 to 2018 due to deforestation to agriculture. The map is aggregated to 9 km spatial resolution for visualization purposes.

Table 2
Global SE change between 2001 and 2012. AGR: Agriculture, FOR: Forest.

SE	AGR-AGR	FOR-FOR	FOR-AGR	AGR-FOR
Rate (Mg ha^{-1}yr^{-1})	0.23	0.041	0.71	0.095
Total (Unit: Gt)	3.2	1.1	0.14	0.018

other locations, such as India, Europe, East China and Southeast Brazil, where natural revegetation is likely ongoing (Mousivand and Arsanjani, 2019). Settlement expanded almost linearly during the entire study period, mainly at the cost of agricultural land. Further, the continuing trends in losses of forests and shrubland for agricultural expansion has high risks for irreversible species loss, especially in areas with highly fragmented habitats, such as the biodiversity hotspots (Betts et al., 2017; Barlow et al., 2016). Due to climate warming, wetland at high latitude is decreasing, and it is mainly replaced by forests (Zhu et al., 2016). We found greening trends for bare areas, with increasing presence of grass and sparse vegetation because of CO_2 fertilization and other climate feedbacks (Zhu et al., 2016). On the other hand, human effects of conservation activities and forestry can lead to large scale expansion of forests, such as in Southern China and coastal Brazil (Brandt et al., 2018).

Our analysis also showed an example of the importance of changes in land covers for key global environmental processes, such as soil erosion and carbon emissions, thanks to the integration of the land cover products with other datasets of terrestrial ecosystem properties. We estimated global annual ABC loss due to deforestation from expansion of agriculture and settlement of 1.2 (0.7/1.4) GtC/yr, which is of 1.5 (1.0/1.8) GtC/yr when BBC is included. In the tropics, values are of 1.0 (0.6/1.3) GtC/yr when both ABC and BBC are considered. These are gross estimates of carbon losses from vegetation due to major drivers (i.e., expansion of agriculture and urban areas), which do not rely on specific assumptions about the fate of converted forestland or harvested wood products. A comparison with existing studies is challenging, especially at global levels, owing to different approaches, spatial scales, temporal periods, and types of processes considered (Zarin, 2012; Ramankutty et al., 2007). Harris et al. (2012) estimated an average gross carbon loss of 0.81 GtC/yr using satellite observations of deforestation in the tropics from 2000 to 2005, including both above- and below-ground biomass carbon. Their outcomes are 25–50% of recently published estimates. Baccini et al. (2017) estimated changes of carbon in woody vegetation from deforestation and forest degradation in the tropical region and reported an average loss of 0.86 GtC/yr from 2003 to 2014 using the MODIS

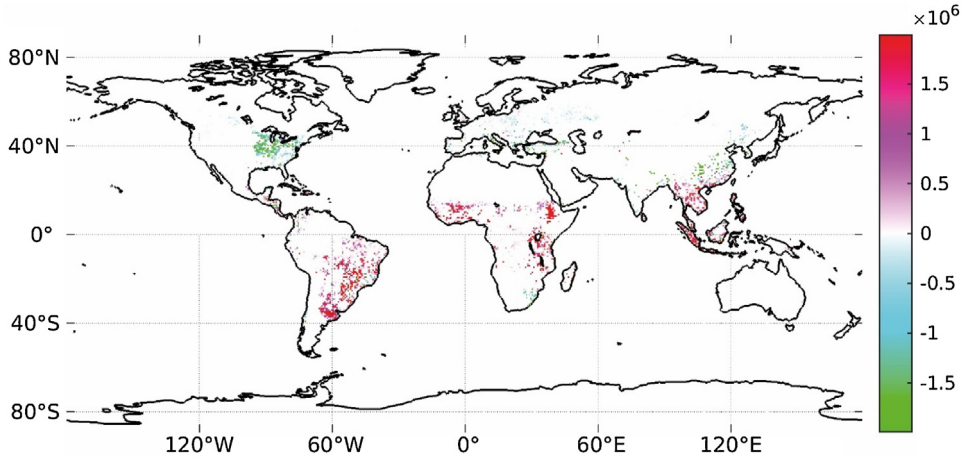

Fig. 7. Spatial pattern of differences in global soil erosion rates between 2001 and 2012 in agricultural land (AGR-AGR). Negative values indicate SE alleviation (i.e., a reduction in SE rate), and positive values SE aggravation. AGR-AGR refers to the grid cells classified as agriculture both in 2001 and 2012 (unit: t). This map is aggregated to 75 km spatial resolution for visualization purposes only.

pantropical satellite data, and argued that emissions from degradation are probably larger than those from deforestation.

Our analysis only accounted for carbon losses from vegetation carbon resulting from transitions from forest cover to agriculture and settlements. Most of the existing global studies produced estimates that include a variety of other processes, such as changes in soil organic carbon, forest growth or degradation, and expansion of new forests, so reporting net emissions from changes in land use. For example, Houghton and Nassikas (2017) estimated a global net carbon emission from land use changes during 2006–2015 of 1.1 GtC/yr using the bookkeeping model to prescribe vegetation and soil carbon density changes. Le Quéré et al. (2016) reported a global carbon emission of 1.3 GtC/yr during 2006–2015 from an ensemble of land surface models, and Friedlingstein et al. (2019) provided a recent estimate of 1.5 GtC/yr for the period 2009−2018. They both computed carbon fluxes from land use changes and included estimates for both vegetation (deforestation and forest growth/expansion) and soil carbon. All these analyses used the bookkeeping model to prescribe vegetation and soil carbon density changes and land cover data from the Food and Agriculture Organization of the United Nations (Keenan et al., 2015). In the bookkeeping method, there are many broad assumptions about the fate of cleared lands and their respective carbon stocks to estimate the associated net carbon fluxes, which include CO_2 fluxes from deforestation, afforestation, logging (forest degradation and harvest activity), shifting cultivation, and regrowth of forests following wood harvest or abandonment of agriculture.

Our analysis did not attempt to estimate soil emissions, but the soil carbon pool is much larger than the carbon in living biomass. However, the effects of land use changes on soil carbon emissions are difficult to quantify and still poorly understood (Guo and Gifford, 2002; Don et al., 2011). Existing estimates typically rely on default factors that approximate soil carbon from aboveground biomass densities (Pan et al., 2011), but these factors highly vary across ecosystems and climates (Piao et al., 2009; Duarte-Guardia et al., 2019). For example, global and regional meta-analysis of field measurements find that soil organic carbon can either increase, decrease, or remain constant after afforestation, because the soil carbon response is sensitive to the interactions of multiple local factors, such as tree species, previous land use, initial soil carbon content, stand age, climate and soil type (Hong et al., 2020). Our analysis also treated all carbon losses from forest clearance as instantaneous emissions, without considering potential storage of carbon in harvested wood products or forest remaining forest after the disturbance (i.e., forest management, which is common in the Northern hemisphere) (Iordan et al., 2018; Ceccherini et al., 2020; Cherubini et al., 2016). Alternative emission estimates require assumptions about the fate of converted lands and biomass harvested, which currently cannot be ascertained with statistical confidence across the globe. If a robust method would allow for the consideration of these data, the result would be a reduction in our estimates of carbon losses.

Changes in land cover is the one of the main drivers of SE (Borrelli et al., 2017), and a better understanding of trends and spatial patterns of SE for different land uses can support local policies aiming at maintaining soil quality and preventing land degradation. We found high SE rates on agriculture land in the tropics, where current agricultural practices are accelerating SE due to unsustainable management practices, such as tillage and over-grazing (Borrelli et al., 2017; Montgomery, 2007). More conservation practices are needed in these countries to preserve soil layers. Our findings of 5.2 Mg ha^{-1} yr^{-1} in 2012 of SE rates on agricultural land are in line with Nearing et al. (2017a), which reported a value of global average SE rate on cropland with traditional tillage of 5.7 Mg ha^{-1} yr^{-1}. However, we found smaller rates of SE than the findings of Borrelli et al. (2017), which estimated SE rates on cropland to be much higher than the global average soil erosion rate. This might be due to different resolution of the data used (25 km vs. 250 m), and to possible inconsistencies in classification of land use types across the land use and the SE datasets.

Land cover change is an indicator for assessing the threat to biodiversity, even though the implications are highly dependent on the local context (Uchida and Ushimaru, 2014; Strassburg et al., 2020). Agriculture expansion on forest and other land covers challenges biodiversity conservation, especially in biodiversity hotspots and intact landscape (Betts et al., 2017). Our results reveal that significant changes occurred at the borders of pristine areas, such as the Amazon rainforest, the tropical forests of Central-east Africa, and the Brazilian Cerrado (shrubland), with high potential risks for species loss (Hu et al., 2020). This trend calls for global attention to make the today's agri-food sector more efficient and to adopt more sustainable diets, so to alleviate pressure from deforestation and prevent further habitat conversion (Folberth et al., 2020; McElwee et al., 2020). Otherwise, the expected rising demands for food and feed for an always increasing population will continue to drive expansion of agriculture land at expenses of natural areas (IPCC, 2019).

5. Conclusions

We combined the ESA−CCI land cover product with the newly released C3S-CDS land cover product to study their representation of recent historical land cover dynamics by retaining the original high spatial resolution (300 m) of the datasets. We further integrated these products with global datasets of biomass carbon density and SE rate to answer the research questions raised in the introduction section.

- We found that 5.5 % of the total ice-free land surface transitioned to a different land cover from 1992 to 2018. The major expansions are registered for settlements (+44 Mha, the largest relative increase) and agriculture (+79 Mha), while declines are observed for wetland (−11 Mha, the largest relative decrease), forests (-45 Mha), shrubland (−33 Mha) and bare land (-29 Mha). Declines in forest areas mostly occurred before 1999, but they are still ongoing today (although net changes are small because of contrasting trends of forest expansion). The main transitions involved are expansion of agricultural land into forestland or shrubland, afforestation of agricultural land or shrubland, greening of bare land and wetland drying to forests or sparse vegetation. Most of these transitions are the results of anthropogenic activities, either directly through land use (i.e., deforestation for agricultural expansion) or indirectly via well-known climate change feedbacks (i.e., vegetation enhancement or wetland drying in boreal ecosystems).
- Clear spatial patterns emerged for the major historical land transitions. For example, agriculture expansion at expenses of forests or shrubland mainly happened at the borders of the Amazon basin, in Southeast Asia, Eastern Asia, US, and Central Africa. Afforestation is mainly found in association with either cropland abandonment due to socio-economic reasons, such as in Eastern Europe, or for ecological restoration to contrast land degradation, such as in coastal Brazil and China. Settlement expansion mostly occurred in Eastern China, India, US, and Western Europe. In northern or mountainous ecosystems, we found that climate feedbacks are favoring the transition of sparse vegetation to forests, greening of bare land, and wetland drying.
- We found important contributions from recent land use and land cover changes to key global environmental processes, such as gross carbon losses from vegetation clearance and effects on soil erosion rates. Between 2010 and 2018, we estimated that an

average of 11.7 GtC are emitted from deforestation driven by agriculture expansion, and 0.33 GtC are released from conversion of forest to settlements. There has been increases in soil erosion rates at a global level (from 5.0 Mg ha^{-1} yr^{-1} in 2001 to 5.2 Mg ha^{-1} yr^{-1} in 2012), but with large differences by type of land use and land transition. The transition from forest to agriculture showed the largest soil erosion rates, while forest areas have the smallest rates of soil loss. Agricultural land that remained agriculture had approximately one third of the erosion rate per hectare of deforested land, but it had the largest total soil loss due to the large areas of cultivated land on the planet. Afforestation resulted as an effective measure to decrease rates of soil erosion.

The results of this study show a human-dominated Earth system. Direct human-induced land use and land cover changes are observed over large areas on every continent, with implications for maintaining ecosystem services. The well documented indirect human-induced effects on land cover are also found to be the driver of large-scale regional land dynamics, which include greening processes, woody encroachment in boreal and montane systems, wetland drying and vegetation loss in semi-arid areas. These ongoing trends in land-use change and the increasing contributions of climate change in altering land covers requires expanding efforts for monitoring the Earth's land surface and better understanding its interlinkages with key environmental processes.

In addition to further increase the accuracy of datasets of land cover classes (Bayer et al., 2020), possible extensions of this work include the possibility to integrate maps of land covers with other datasets of environmental attributes, as here exemplified with biomass carbon and SE, as well as support the prediction of future land cover dynamics based on historical trends, ideally by coupling with key indicators of socio-economic development and climate change (Chen et al., 2020; Hurtt et al., 2020). Overall, a better understanding of land cover dynamics and their interlinkages to key environmental mechanisms ultimately helps shaping beneficial land use strategies that contribute to achieve synergies among different Sustainable Development Goals, such as "Climate Action", "Life on Land", "Clean water and sanitation", and "Zero Hunger". For example, the bottom-up approach used in this work showed accelerated rates of SE due to agriculture activities in several developing countries, which can lead to soil degradation, farmer income insecurity and deforestation for establishing new crop plantations in more fertile soils. The successful identification of areas at risks of soil erosion and possible mitigation measures thus requires integrated policies at the interface of geography, climate and social sciences.

Declaration of Competing Interest

The authors report no declarations of interest.

Acknowledgements

X.H. and F.C. acknowledge the support of the Norwegian Research Council through the project MitiStress (project no. 286773), and. W.Z. acknowledges support from the National Natural Science Foundation of China (project no. 41861134038). We also acknowledge the ESA and C3S for the land cover product, Borrelli et al. (2017) for the soil erosion dataset, and Spawn et al. (2020) for the aboveground biomass carbon density dataset.

Appendix A. Supplementary data

Supplementary material related to this article can be found, in the online version, at doi:https://doi.org/10.1016/j.ancene.2021.100291.

References

Alkama, R., Cescatti, A., 2016. Biophysical climate impacts of recent changes in global forest cover. Science 351, 600–604.
Arsanjani, J.J., Helbich, M., Vaz, E.D., 2013. Spatiotemporal simulation of urban growth patterns using agent-based modeling: the case of Tehran. Cities 32, 33–42.
Arsanjani, J.J., Fibaek, C.S., Vaz, E., 2018. Development of a cellular automata model using open source technologies for monitoring urbanisation in the global south: The case of Maputo, Mozambique. Habitat Int. 71, 38–48.
Baccini, A., Walker, W., Carvalho, L., Farina, M., Sulla-Menashe, D., Houghton, R., 2017. Tropical forests are a net carbon source based on aboveground measurements of gain and loss. Science 358, 230–234.
Bagarello, V., Di Stefano, C., Ferro, V., Pampalone, V., 2017. Predicting maximum annual values of event soil loss by USLE-type models. Catena 155, 10–19.
Bailey, K.M., Mccleery, R.A., Binford, M.W., Zweig, C., 2016. Land-cover change within and around protected areas in a biodiversity hotspot. J. Land Use Sci. 11, 154–176.
Barlow, J., Lennox, G.D., Ferreira, J., Berenguer, E., Lees, A.C., Mac Nally, R., Thomson, J.R., De Barros Ferraz, S.F., Louzada, J., Oliveira, V.H.F., 2016. Anthropogenic disturbance in tropical forests can double biodiversity loss from deforestation. Nature 535, 144–147.
Bayer, A.D., Fuchs, R., Mey, R., Krause, A., Verburg, P.H., Anthoni, P., Arneth, A., 2020. Diverging land-use projections cause large variability in their impacts on ecosystems and related indicators for ecosystem services. Earth Syst. Dyn. Discuss. 1–32.
Bestelmeyer, B.T., Okin, G.S., Duniway, M.C., Archer, S.R., Sayre, N.F., Williamson, J.C., Herrick, J.E., 2015. Desertification, land use, and the transformation of global drylands. Front. Ecol. Environ. 13, 28–36.
Betts, M.G., Wolf, C., Ripple, W.J., Phalan, B., Millers, K.A., Duarte, A., Butchart, S.H., Levi, T., 2017. Global forest loss disproportionately erodes biodiversity in intact landscapes. Nature 547, 441–444.
Bonan, G.B., 2008. Forests and climate change: forcings, feedbacks, and the climate benefits of forests. Science 320, 1444–1449.
Borrelli, P., Robinson, D.A., Fleischer, L.R., Lugato, E., Ballabio, C., Alewell, C., Meusburger, K., Modugno, S., Schutt, B., Ferro, V., Bagarello, V., Van Oost, K., Montanarella, L., Panagos, P., 2017. An assessment of the global impact of 21st century land use change on soil erosion. Nat. Commun. 8, 1–13.
Borrelli, P., Robinson, D.A., Panagos, P., Lugato, E., Yang, J.E., Alewell, C., Wuepper, D., Montanarella, L., Ballabio, C., 2020. Land use and climate change impacts on global soil erosion by water (2015-2070). Proc. Natl. Acad. Sci. 117, 21994–22001.
Brandt, M., Yue, Y.M., Wigneron, J.P., Tong, X.W., Tian, F., Jepsen, M.R., Xiao, X.M., Verger, A., Mialon, A., Al-Yaari, A., Wang, K.L., Fensholt, R., 2018. Satellite-observed major greening and biomass increase in South China karst during recent decade. Earths Future 6, 1017–1028.
C3S, 2019. Land Cover Classification Gridded Maps From 1992 to Present Derived From Satellite Observations. [Online]. Available: https://cds.climate.copernicus.eu/cdsapp#!/dataset/satellite-land-cover?tab=overview [Accessed 05.07 2020]. .
Cakir, G., Un, C., Baskent, E.Z., Kose, S., Sivrikaya, F., Keles, S., 2008. Evaluating urbanization, fragmentation and land Use/Land cover change pattern in Istanbul City, Turkey from 1971 to 2002. Land Degrad. Dev. 19, 663–675.
Ceccherini, G., Duveiller, G., Grassi, G., Lemoine, G., Avitabile, V., Pilli, R., Cescatti, A., 2020. Abrupt increase in harvested forest area over Europe after 2015. Nature 583, 72–77.
Chen, W., Chi, G., Li, J., 2019. The spatial association of ecosystem services with land use and land cover change at the county level in China, 1995–2015. Sci. Total Environ. 669, 459–470.
Chen, M., Vernon, C.R., Graham, N.T., Hejazi, M., Huang, M., Cheng, Y., Calvin, K., 2020. Global land use for 2015–2100 at 0.05° resolution under diverse socioeconomic and climate scenarios. Sci. Data 7, 1–11.
Cherubini, F., Huijbregts, M., Kindermann, G., Van Zelm, R., Van Der Velde, M., Stadler, K., Strømman, A.H., 2016. Global spatially explicit CO 2 emission metrics for forest bioenergy. Sci. Rep. 6, 1–12.
Cherubini, F., Huang, B., Hu, X.P., Tolle, M.H., Stromman, A.H., 2018a. Quantifying the climate response to extreme land cover changes in Europe with a regional model. Environ. Res. Lett. 13, 074002.
Cherubini, F., Santaniello, F., Hu, X.P., Sonesson, J., Stromman, A.H., Weslien, J., Djupstrom, L.B., Ranius, T., 2018b. Climate impacts of retention forestry in a Swedish boreal pine forest. J. Land Use Sci. 13, 301–318.
Debanshi, S., Pal, S., 2020. Wetland delineation simulation and prediction in deltaic landscape. Ecol. Indic. 108, 105757.
Defourny, P., Schouten, L., Bartalev, S., Bontemps, S., Cacetta, P., De Wit, A., Di Bella, C., Gérard, B., Giri, C., Gond, V., 2009. Accuracy Assessment of a 300 M Global Land Cover Map: the GlobCover Experience. .
Di Gregorio, A., 2016. Land Cover Classification System: Classification Concepts. Food and Agriculture Organization of the United Nations, Rom, Italy.
Don, A., Schumacher, J., Freibauer, A., 2011. Impact of tropical land-use change on soil organic carbon stocks–a meta-analysis. Glob. Chang. Biol. 17, 1658–1670.
Duarte-Guardia, S., Peri, P.L., Amelung, W., Sheil, D., Laffan, S.W., Borchard, N., Bird, M.I., Dieleman, W., Pepper, D.A., Zutta, B., 2019. Better estimates of soil carbon from geographical data: a revised global approach. Mitig. Adapt. Strateg. Glob. Chang. 24, 355–372.
Duveiller, G., Hooker, J., Cescatti, A., 2018. The mark of vegetation change on Earth's surface energy balance. Nat. Commun. 9, 679.
Duveiller, G., Caporaso, L., Abad-Viñas, R., Perugini, L., Grassi, G., Arneth, A., Cescatti, A., 2020. Local biophysical effects of land use and land cover change: towards an assessment tool for policy makers. Land Use Policy 91, 104382.

Ellis, E.C., Ramankutty, N., 2008. Putting people in the map: anthropogenic biomes of the world. Front. Ecol. Environ. 6, 439–447.
Englund, O., Borjesson, P., Berndes, G., Scarlat, N., Dallemand, J.F., Grizzetti, B., Dimitriou, I., Mola-Yudego, B., Fahl, F., 2020. Beneficial land use change: strategic expansion of new biomass plantations can reduce environmental impacts from EU agriculture. Glob. Environ. Change 60, 101990.
ESA, 2017. Land Cover CCI: Product User Guide Version 2.0. [Online]. Available: https://maps.elie.ucl.ac.be/CCI/viewer/download/ESACCI-LC-Ph2-PUGv2_2.0.pdf [Accessed May, 27th 2020]. .
Feng, X., Fu, B., Piao, S., Wang, S., Ciais, P., Zeng, Z., Lü, Y., Zeng, Y., Li, Y., Jiang, X., 2016. Revegetation in China's Loess Plateau is approaching sustainable water resource limits. Nat. Clim. Chang. 6, 1019–1022.
Feng, Q., Zhao, W., Hu, X., Liu, Y., Daryanto, S., Cherubini, F., 2020. Trading-off ecosystem services for better ecological restoration: a case study in the Loess Plateau of China. J. Clean. Prod. 257, 120469.
Folberth, C., Khabarov, N., Balkovič, J., Skalský, R., Visconti, P., Ciais, P., Janssens, I.A., Peñuelas, J., Obersteiner, M., 2020. The global cropland-sparing potential of high-yield farming. Nat. Sustain. 3, 281–289.
Foley, J.A., Defries, R., Asner, G.P., Barford, C., Bonan, G., Carpenter, S.R., Chapin, F.S., Coe, M.T., Daily, G.C., Gibbs, H.K., Helkowski, J.H., Holloway, T., Howard, E.A., Kucharik, C.J., Monfreda, C., Patz, J.A., Prentice, I.C., Ramankutty, N., Snyder, P.K., 2005. Global consequences of land use. Science 309, 570–574.
Friedlingstein, P., Jones, M.W., O'sullivan, M., Andrew, R.M., Hauck, J., Peters, G.P., Peters, W., Pongratz, J., Sitch, S., Le Quere, C., Bakker, D.C.E., Canadell, J.G., Ciais, P., Jackson, R.B., Anthoni, P., Barbero, L., Bastos, A., Bastrikov, V., Becker, M., Bopp, L., Buitenhuis, E., Chandra, N., Chevallier, F., Chini, L.P., Currie, K.I., Feely, R.A., Gehlen, M., Gilfillan, D., Gkritzalis, T., Goll, D.S., Gruber, N., Gutekunst, S., Harris, I., Haverd, V., Houghton, R.A., Hurtt, G., Ilyina, T., Jain, A.K., Joetzjer, E., Kaplan, J. O., Kato, E., Goldewijk, K.K., Korsbakken, J.I., Landschutzer, P., Lauvset, S.K., Lefevre, N., Lenton, A., Lienert, S., Lombardozzi, D., Marland, G., Mcguire, P.C., Melton, J.R., Metzl, N., Munro, D.R., Nabel, J.E.M.S., Nakaoka, S.I., Neill, C., Omar, A.M., Ono, T., Peregon, A., Pierrot, D., Poulter, B., Rehder, G., Resplandy, L., Robertson, E., Rodenbeck, C., Seferian, R., Schwinger, J., Smith, N., Tans, P.P., Tian, H.Q., Tilbrook, B., Tubiello, F.N., Van Der Werf, G.R., Wiltshire, A.J., Zaehle, S., 2019. Global carbon budget 2019. Earth Syst. Sci. Data 11, 1783–1838.
Ghosh, S., Dinda, S., Das Chatterjee, N., Das, K., 2018. Analyzing risk factors for shrinkage and transformation of East Kolkata Wetland, India. Spat. Inf. Res. 26, 661–677.
Grau, H.R., Gasparri, N.I., Aide, T.M., 2005. Agriculture expansion and deforestation in seasonally dry forests of north-west Argentina. Environ. Conserv. 32, 140–148.
Green, A.J., Alcorlo, P., Peeters, E.T., Morris, E.P., Espinar, J.L., Bravo-Utrera, M.A., Bustamante, J., Díaz-Delgado, R., Koelmans, A.A., Mateo, R., 2017. Creating a safe operating space for wetlands in a changing climate. Front. Ecol. Environ. 15, 99–107.
Guo, L.B., Gifford, R.M., 2002. Soil carbon stocks and land use change: a meta analysis. Glob. Chang. Biol. 8, 345–360.
Hansen, M.C., Potapov, P.V., Moore, R., Hancher, M., Turubanova, S.A., Tyukavina, A., Thau, D., Stehman, S., Goetz, S.J., Loveland, T.R., 2013. High-resolution global maps of 21st-century forest cover change. science 342, 850–853.
Harris, N.L., Brown, S., Hagen, S.C., Saatchi, S.S., Petrova, S., Salas, W., Hansen, M.C., Potapov, P.V., Lotsch, A., 2012. Baseline map of carbon emissions from deforestation in tropical regions. Science 336, 1573–1576.
Hong, S., Yin, G., Piao, S., Dybzinski, R., Cong, N., Li, X., Wang, K., Peñuelas, J., Zeng, H., Chen, A., 2020. Divergent responses of soil organic carbon to afforestation. Nat. Sustain. 3, 694–700.
Hou, W., Hou, X., 2019. Data fusion and accuracy analysis of multi-source land Use/Land cover datasets along coastal areas of the maritime silk road. ISPRS Int. J. Geoinf. 8, 557.
Houghton, R.A., Nassikas, A.A., 2017. Global and regional fluxes of carbon from land use and land cover change 1850–2015. Global Biogeochem. Cycles 31, 456–472.
Hu, X.P., Huang, B., Cherubini, F., 2019. Impacts of idealized land cover changes on climate extremes in Europe. Ecol. Indic. 104, 626–635.
Hu, X., Huang, B., Verones, F., Cavalett, O., Cherubini, F., 2020. Overview of recent land cover changes in biodiversity hotspots. Front. Ecol. Environ. 7.
Hua, T., Zhao, W.W., Liu, Y.X., Wang, S., Yang, S.Q., 2018. Spatial consistency assessments for global land-cover datasets: a comparison among GLC2000, CCI LC, MCD12, GLOBCOVER and GLCNMO. Remote Sens. (Basel) 10, 1846.
Huang, B., Hu, X.P., Fuglstad, G.A., Zhou, X., Zhao, W.W., Cherubini, F., 2020a. Predominant regional biophysical cooling from recent land cover changes in Europe. Nat. Commun. 11, 1–13.
Huang, C., Zhou, Z., Teng, M., Wu, C., Wang, P., 2020b. Effects of climate, land use and land cover changes on soil loss in the Three Gorges Reservoir area, China. Geography and Sustainability 1, 200–208.
Hurtt, G.C., Chini, L.P., Frolking, S., Betts, R.A., Feddema, J., Fischer, G., Fisk, J.P., Hibbard, K., Houghton, R.A., Janetos, A., Jones, C.D., Kindermann, G., Kinoshita, T., Goldewijk, K.K., Riahi, K., Shevliakova, E., Smith, S., Stehfest, E., Thomson, A., Thornton, P., Van Vuuren, D.P., Wang, Y.P., 2011. Harmonization of land-use scenarios for the period 1500-2100: 600 years of global gridded annual land-use transitions, wood harvest, and resulting secondary lands. Clim. Change 109, 117–161.
Hurtt, G.C., Chini, L., Sahajpal, R., Frolking, S., Bodirsky, B.L., Calvin, K., Doelman, J.C., Fisk, J., Fujimori, S., Goldewijk, K.K., 2020. Harmonization of global land-use change and management for the period 850–2100 (LUH2) for CMIP6. Geosci. Model. Dev. Discuss. 1–65.
Iordan, C.M., Hu, X., Arvesen, A., Kauppi, P., Cherubini, F., 2018. Contribution of forest wood products to negative emissions: historical comparative analysis from 1960 to 2015 in Norway, Sweden and Finland. Carbon Balance Manag. 13, 12.
IPCC, 2019. Summary for Policymakers. In: Shukla, P.R., Skea, J., Calvo Buendia, E., Masson-Delmotte, V., Pörtner, H.-O., Roberts, D.C., Zhai, P., Slade, R., Connors, S., van Diemen, R., Ferrat, M., Haughey, E., Luz, S., Neogi, S., Pathak, M., Petzold, J., Portugal Pereira, J., Vyas, P., Huntley, E., Kissick, K., Belkacemi, M., Malley, J. (Eds.), Climate Change and Land: an IPCC Special Report on Climate Change, Desertification, Land Degradation, Sustainable Land Management, Food Security, and Greenhouse Gas Fluxes in Terrestrial Ecosystems, In press.
Jaimes, N.B.P., Sendra, J.B., Delgado, M.G., Plata, R.F., 2010. Exploring the driving forces behind deforestation in the state of Mexico (Mexico) using geographically weighted regression. Appl. Geogr. 30, 576–591.
Keenan, R.J., Reams, G.A., Achard, F., De Freitas, J.V., Grainger, A., Lindquist, E., 2015. Dynamics of global forest area: results from the FAO global forest resources assessment 2015. For. Ecol. Manage. 352, 9–20.
Klein Goldewijk, K., Beusen, A., Doelman, J., Stehfest, E., 2017. Anthropogenic land use estimates for the Holocene–HYDE 3.2. Earth Syst. Sci. Data Discuss. 9, 927–953.
Krause, M., Lotze-Campen, H., Popp, A., 2009. Spatially-explicit Scenarios on Global Cropland Expansion and Available Forest Land in an Integrated Modelling Framework. .
Kuemmerle, T., Levers, C., Erb, K., Estel, S., Jepsen, M.R., Müller, D., Plutzar, C., Stürck, J., Verkerk, P.J., Verburg, P.H., 2016. Hotspots of land use change in Europe. Environ. Res. Lett. 11, 064020.
Lamchin, M., Lee, J.Y., Lee, W.K., Lee, E.J., Kim, M., Lim, C.H., Choi, H.A., Kim, S.R., 2016. Assessment of land cover change and desertification using remote sensing technology in a local region of Mongolia. Adv. Space Res. 57, 64–77.
Le Quéré, C., Andrew, R., Canadell, J.G., Sitch, S., Korsbakken, J.I., Peters, G.P., Manning, A.C., Boden, T.A., Tans, P.P., Houghton, R.A., 2016. Global Carbon Budget 2016. .
Leirpoll, M.E., Næss, J.S., Cavalett, O., Dorber, M., Hu, X., Cherubini, F., 2021. Optimal combination of bioenergy and solar photovoltaic for renewable energy production on abandoned cropland. Renew. Energy 168, 45–56.
Lejeune, Q., Davin, E.L., Gudmundsson, L., Winckler, J., Seneviratne, S.I., 2018. Historical deforestation locally increased the intensity of hot days in northern mid-latitudes. Nat. Clim. Chang. 8, 386–+.
Lepers, E., Lambin, E.F., Janetos, A.C., Defries, R., Achard, F., Ramankutty, N., Scholes, R.J., 2005. A synthesis of information on rapid land-cover change for the period 1981-2000. Bioscience 55, 115–124.
Lesiv, M., Schepaschenko, D., Moltchanova, E., Bun, R., Dürauer, M., Prishchepov, A. V., Schierhorn, F., Estel, S., Kuemmerle, T., Alcántara, C., 2018. Spatial distribution of arable and abandoned land across former Soviet Union countries. Sci. Data 5, 180056.
Li, W., Ciais, P., Macbean, N., Peng, S.S., Defourny, P., Bontemps, S., 2016. Major forest changes and land cover transitions based on plant functional types derived from the ESA CCI Land Cover product. Int. J. Appl. Earth Obs. Geoinf. 47, 30–39.
Li, W., Macbean, N., Ciais, P., Defourny, P., Lamarche, C., Bontemps, S., Houghton, R.A., Peng, S.S., 2018. Gross and net land cover changes in the main plant functional types derived from the annual ESA CCI land cover maps (1992-2015). Earth Syst. Sci. Data 10, 219–234.
Liang, L., Liu, Q., Liu, G., Li, H., Huang, C., 2019. Accuracy evaluation and consistency analysis of four global land cover products in the Arctic Region. Remote Sens. (Basel) 11, 1396.
Liu, X.X., Yu, L., Li, W., Peng, D.L., Zhong, L.H., Li, L., Xin, Q.C., Lu, H., Yu, C.Q., Gong, P., 2018a. Comparison of country-level cropland areas between ESA-CCI land cover maps and FAOSTAT data. Int. J. Remote Sens. 39, 6631–6645.
Liu, X.X., Yu, L., Si, Y.L., Zhang, C., Lu, H., Yu, C.Q., Gong, P., 2018b. Identifying patterns and hotspots of global land cover transitions using the ESA CCI Land Cover dataset. Remote. Sens. Lett. 9, 972–981.
Mcelwee, P., Calvin, K., Campbell, D., Cherubini, F., Grassi, G., Korotkov, V., Le Hoang, A., Lwasa, S., Nkem, J., Nkonya, E., 2020. The impact of interventions in the global land and agri-food sectors on nature's contributions to people and the UN sustainable development goals. Glob. Chang. Biol. 26, 4691–4721.
Montgomery, D.R., 2007. Soil erosion and agricultural sustainability. Proc. Natl. Acad. Sci. U.S.A. 104, 13268–13272.
Mousivand, A., Arsanjani, J.J., 2019. Insights on the historical and emerging global land cover changes: the case of ESA-CCI-LC datasets. Appl. Geogr. 106, 82–92.
Næss, J.S., Cavalett, O., Cherubini, F., 2021. The land–energy–water nexus of global bioenergy potentials from abandoned cropland. Nat. Sustain..
Nearing, M.A., Xie, Y., Liu, B., Ye, Y., 2017a. Natural and anthropogenic rates of soil erosion. Int. Soil Water Conserv. Res. 5, 77–84.
Nearing, M.A., Yin, S.Q., Borrelli, P., Polyakov, V.O., 2017b. Rainfall erosivity: an historical review. Catena 157, 357–362.
Nowosad, J., Stepinski, T.F., Netzel, P., 2019. Global assessment and mapping of changes in mesoscale landscapes: 1992-2015. Int. J. Appl. Earth Obs. Geoinf. 78, 332–340.
Pan, Y., Birdsey, R.A., Fang, J., Houghton, R., Kauppi, P.E., Kurz, W.A., Phillips, O.L., Shvidenko, A., Lewis, S.L., Canadell, J.G., 2011. A large and persistent carbon sink in the world's forests. Science 333, 988–993.
Peng, S.-S., Piao, S., Zeng, Z., Ciais, P., Zhou, L., Li, L.Z., Myneni, R.B., Yin, Y., Zeng, H., 2014. Afforestation in China cools local land surface temperature. Proc. Natl. Acad. Sci. 111, 2915–2919.
Pérez-Hoyos, A., Rembold, F., Kerdiles, H., Gallego, J., 2017. Comparison of global land cover datasets for cropland monitoring. Remote Sens. (Basel) 9, 1118.

Piao, S., Fang, J., Ciais, P., Peylin, P., Huang, Y., Sitch, S., Wang, T., 2009. The carbon balance of terrestrial ecosystems in China. Nature 458, 1009–1013.
Poulter, B., Macbean, N., Hartley, A., Khlystova, I., Arino, O., Betts, R., Bontemps, S., Boettcher, M., Brockmann, C., Defourny, P., 2015. Plant functional type classification for earth system models: results from the European Space Agency's Land Cover Climate Change Initiative. Geosci. Model. Dev. 8, 2315–2328.
Prestele, R., Arneth, A., Bondeau, A., De Noblet-Ducoudré, N., Pugh, T.A., Sitch, S., Stehfest, E., Verburg, P.H., 2017. Current challenges of implementing anthropogenic land-use and land-cover change in models contributing to climate change assessments. Earth Syst. Dyn. 8, 369–386.
Qin, Y., Xiao, X., Dong, J., Zhang, Y., Wu, X., Shimabukuro, Y., Arai, E., Biradar, C., Wang, J., Zou, Z., 2019. Improved estimates of forest cover and loss in the Brazilian Amazon in 2000–2017. Nat. Sustain. 2, 764–772.
Ramankutty, N., Gibbs, H.K., Achard, F., Defries, R., Foley, J.A., Houghton, R., 2007. Challenges to estimating carbon emissions from tropical deforestation. Glob. Chang. Biol. 13, 51–66.
Rezende, C., Scarano, F., Assad, E., Joly, C., Metzger, J., Strassburg, B., Tabarelli, M., Fonseca, G., Mittermeier, R., 2018. From hotspot to hopespot: an opportunity for the Brazilian Atlantic Forest. Perspect. Ecol. Conserv. 16, 208–214.
Risse, L.M., Nearing, M.A., Nicks, A.D., Laflen, J.M., 1993. Error assessment in the universal soil loss equation. Soil Sci. Soc. Am. J. 57, 825–833.
Seneviratne, S.I., Phipps, S.J., Pitman, A.J., Hirsch, A.L., Davin, E.L., Donat, M.G., Hirschi, M., Lenton, A., Wilhelm, M., Kravitz, B., 2018. Land radiative management as contributor to regional-scale climate adaptation and mitigation. Nat. Geosci. 11, 88–+.
Seto, K.C., Güneralp, B., Hutyra, L.R., 2012. Global forecasts of urban expansion to 2030 and direct impacts on biodiversity and carbon pools. Proc. Natl. Acad. Sci. 109, 16083–16088.
Smith, P., Calvin, K., Nkem, J., Campbell, D., Cherubini, F., Grassi, G., Korotkov, V., Le Hoang, A., Lwasa, S., Mcelwee, P., 2020. Which practices co-deliver food security, climate change mitigation and adaptation, and combat land degradation and desertification? Glob. Chang. Biol. 26, 1532–1575.
Song, K., Wang, Z., Li, L., Tedesco, L., Li, F., Jin, C., Du, J., 2012. Wetlands shrinkage, fragmentation and their links to agriculture in the Muleng-Xingkai Plain, China. J. Environ. Manage. 111, 120–132.
Song, X.-P., Hansen, M.C., Stehman, S.V., Potapov, P.V., Tyukavina, A., Vermote, E.F., Townshend, J.R., 2018. Global land change from 1982 to 2016. Nature 560, 639–643.
Spawn, S., Gibbs, H., 2020. Global Aboveground and Belowground Biomass Carbon Density Maps for the Year 2010. doi:http://dx.doi.org/10.3334/ORNLDAAC/1763 [Online]. Available: [Accessed June, 25th 2020].
Spawn, S.A., Lark, T.J., Gibbs, H.K., 2019. Carbon emissions from cropland expansion in the United States. Environ. Res. Lett. 14, 045009.
Spawn, S.A., Sullivan, C.C., Lark, T.J., Gibbs, H.K., 2020. Harmonized global maps of above and belowground biomass carbon density in the year 2010. Sci. Data 7, 1–22.
Stolpe, N.B., 2005. A comparison of the RUSLE, EPIC and WEPP erosion models as calibrated to climate and soil of south-central Chile. Acta Agric. Scand. B Soil Plant Sci. 55, 2–8.
Strassburg, B.B., Iribarrem, A., Beyer, H.L., Cordeiro, C.L., Crouzeilles, R., Jakovac, C.C., Junqueira, A.B., Lacerda, E., Latawiec, A.E., Balmford, A., 2020. Global priority areas for ecosystem restoration. Nature 1–6.
Tarolli, P., Straffelini, E., 2020. Agriculture in Hilly and mountainous landscapes: threats, monitoring and sustainable management. Geog. Sust..
Tolessa, T., Senbeta, F., Kidane, M., 2017. The impact of land use/land cover change on ecosystem services in the central highlands of Ethiopia. Ecosyst. Serv. 23, 47–54.
Tschora, H., Cherubini, F., 2020. Co-benefits and trade-offs of agroforestry for climate change mitigation and other sustainability goals in West Africa. Glob. Ecol. Conserv. 22, e00919.
Turner, B.L., Lambin, E.F., Reenberg, A., 2007. The emergence of land change science for global environmental change and sustainability. Proc. Natl. Acad. Sci. U.S.A. 104, 20666–20671.
Uchida, K., Ushimaru, A., 2014. Biodiversity declines due to abandonment and intensification of agricultural lands: patterns and mechanisms. Ecol. Monogr. 84, 637–658.
Venäläinen, A., Lehtonen, I., Laapas, M., Ruosteenoja, K., Tikkanen, O.P., Viiri, H., Ikonen, V.P., Peltola, H., 2020. Climate change induces multiple risks to boreal forests and forestry in Finland: A literature review. Glob. Chang. Biol. 26, 4178–4196.
Verburg, P.H., Neumann, K., Nol, L., 2011. Challenges in using land use and land cover data for global change studies. Glob. Chang. Biol. 17, 974–989.
Veron, S.R., Paruelo, J.M., Oesterheld, M., 2006. Assessing desertification. J. Arid Environ. 66, 751–763.
Werner, B.A., Johnson, W.C., Guntenspergen, G.R., 2013. Evidence for 20th century climate warming and wetland drying in the N orth A merican P rairie P othole R egion. Ecol. Evol. 3, 3471–3482.
Xu, W., Fan, X., Ma, J., Pimm, S.L., Kong, L., Zeng, Y., Li, X., Xiao, Y., Zheng, H., Liu, J., Wu, B., An, L., Zhang, L., Wang, X., Ouyang, Z., 2019. Hidden loss of wetlands in China. Curr. Biol. 29 (3065–3071), e2.
Yang, Y., Xiao, P., Feng, X., Li, H., 2017. Accuracy assessment of seven global land cover datasets over China. ISPRS J. Photogramm. Remote. Sens. 125, 156–173.
Zarin, D.J., 2012. Carbon from tropical deforestation. Science 336, 1518–1519.
Zhu, Z.C., Piao, S.L., Myneni, R.B., Huang, M.T., Zeng, Z.Z., Canadell, J.G., Ciais, P., Sitch, S., Friedlingstein, P., Arneth, A., Cao, C.X., Cheng, L., Kato, E., Koven, C., Li, Y., Lian, X., Liu, Y.W., Liu, R.G., Mao, J.F., Pan, Y.Z., Peng, S.S., Penuelas, J., Poulter, B., Pugh, T.A.M., Stocker, B.D., Viovy, N., Wang, X.H., Wang, Y.P., Xiao, Z.Q., Yang, H., Zaehle, S., Zeng, N., 2016. Greening of the Earth and its drivers. Nat. Clim. Chang. 6 791-+.